

Article

Influence of Fluoroethylene Carbonate in the Composition of an Aprotic Electrolyte on the Electrochemical Characteristics of LIB's Anodes Based on Carbonized Nanosilicon

Alesya V. Parfeneva ¹, Aleksander M. Rumyantsev ¹, Darina A. Lozhkina ¹, Maxim Yu. Maximov ²  and Ekaterina V. Astrova ^{1,*}

¹ Ioffe Institute, Russian Academy of Sciences, Politekhnicheskaya St. 26, 194021 Saint Petersburg, Russia

² Institute of Machinery, Materials and Transport, Peter the Great Saint-Petersburg Polytechnic University, Politekhnicheskaya St. 29, 195251 Saint Petersburg, Russia

* Correspondence: east@mail.ioffe.ru

Abstract: Here, we study an effect of FEC addition to TC-E918 electrolyte on the electrochemical performance of Si/C negative electrodes. The anodes were fabricated from nanosilicon powder coated with a carbon shell by means of a standard slurry technique. The low-temperature reduction of fluorocarbon on the surface of Si nanoparticles was used to form the shell. It was shown that the presence of FEC in the electrolyte increases the cyclic stability of the electrodes and maintains a 1.5-fold higher discharge capacity during 300 cycles. Impedance measurements were used to study changes in the electrode parameters during long-term cycling with and without FEC additives.



Citation: Parfeneva, A.V.; Rumyantsev, A.M.; Lozhkina, D.A.; Maximov, M.Y.; Astrova, E.V. Influence of Fluoroethylene Carbonate in the Composition of an Aprotic Electrolyte on the Electrochemical Characteristics of LIB's Anodes Based on Carbonized Nanosilicon. *Batteries* **2022**, *8*, 91. <https://doi.org/10.3390/batteries8080091>

Academic Editor: Biao Li

Received: 18 July 2022

Accepted: 11 August 2022

Published: 15 August 2022

Publisher's Note: MDPI stays neutral with regard to jurisdictional claims in published maps and institutional affiliations.



Copyright: © 2022 by the authors. Licensee MDPI, Basel, Switzerland. This article is an open access article distributed under the terms and conditions of the Creative Commons Attribution (CC BY) license (<https://creativecommons.org/licenses/by/4.0/>).

1. Introduction

One of the main problems associated with the operation of lithium-ion batteries (LIB) is their cyclic life. This problem is especially relevant for anodes with high specific capacity, such as silicon and its composites. Si forms alloys with a high content of Li, accompanied by a significant change in volume. The resulting mechanical stresses cause destruction of the material and the rapid degradation of the anode. The problem can be partially solved by using nanosized silicon particles [1–3]. The second important factor determining the stability of the electrode operation is the properties of the solid electrolyte interphase (SEI) passivating film, formed on the anode surface as a result of the reduction of the components of the aprotic electrolyte in the first charge cycles [4–6]. The thickness of the SEI layer is several tens of nanometers; it has good permeability for Li ions and plays a protective role in the operation of the electrode [7]. The formation of SEI is determined by the electrode material, its potential, and electrolyte composition [8]. In the case of silicon, more electricity is spent on the formation of SEI than in the case of a traditional graphite anode, which leads to a low columbic efficiency (CE) of the first cycles. In 2006, the first report appeared showing that the addition of 3 wt.% fluoroethylene carbonate (FEC) to a base electrolyte consisting of ethylene carbonate (EC), diethyl carbonate (DEC) (1:1) and 1.3 M LiPF₆ significantly improved the properties of thin-film Si electrode [9]. Further studies [2,10–15] showed that the key role of fluoroethylene carbonate is to change the SEI parameters: to reduce the thickness and increase the uniformity of the film on the silicon surface. This yielded an increase in the discharge capacity, a decrease in the degradation rate, a decrease in irreversible losses and delithiation potential, and an increase in thermal stability.

However, each electrode material and each base electrolyte have their own characteristics, and the FEC additive can affect cell performance in different ways. In this work, we

studied the electrochemical parameters of composite Si/C anodes obtained by reduction of fluorocarbon with silicon. The carbonization method, proposed by us in [16], when the reduction of fluorocarbon by silicon (1) occurs during annealing, made it possible to fabricate porous anodes consisting of spherical Si nanoparticles coated with a carbon shell.



Using different ratios of the initial components Si and $\text{CF}_{0.8}$, composites were obtained and studied mainly in the form of pressed pellets [17]. Here, the anodes were fabricated by the slurry method and studied as a part of a half-cell with a commercial electrolyte TC-E918 (Tinci, China). This electrolyte is suitable for high-voltage cathode materials in order to obtain the high specific energy of a full cell. It was shown in [17] that composites prepared from an initial mixture containing 65–70 wt.% fluorocarbon have optimal electrochemical characteristics. In this case, the reaction product has a composition of 37% Si + 63% C.

In the present research, we studied charge–discharge characteristics, cyclic life, and data of impedance spectroscopy in half-cells using TC-E918 electrolyte with and without FEC additives of the Si/C composite obtained by the new carbonization method during long-term cycling.

2. Materials and Methods

Commercial silicon powder (Hongwu Nanometer, crystalline particles 30–50 nm in diameter) and fluorocarbon $\text{CF}_{0.8}$ (Halopolymer, grains 0.3–5 μm in size) were used to obtain a Si/C composite. The initial powders were taken in the proportion of 35 wt.% Si and 65 wt.% $\text{CF}_{0.8}$, thoroughly mixed and rubbed in an agate mortar. Composite Si/C anodes were produced in two versions: in the form of compressed pellets and in the form of a powder using the standard slurry technology. Silicon carbonization was carried out by annealing pellets or powder in a quasi-closed volume of graphite cassettes. The cassettes were placed in a muffle furnace with a quartz tube purged with high purity argon and heated to 400 °C. After 10 min, the furnace temperature was slowly (during 2 h) raised to 800 °C, followed by holding the sample at this temperature for 20 min and cooling down to 530 °C.

To fabricate an anode, the pellets were glued to a copper foil using a thin layer of a slurry based on polyvinylidene fluoride (PVDF), highly split graphite and NMP (N-methylpyrrolidone). In the case of the slurry technology, a mixture of the composition was the following: composite Si/C:carbon black (C-NERGY SUPER C65):PVDF (Solef 5130,Solvay):VGCF (vapor grown carbon fibers, Showa Denko) = 88:5:5:2 wt.%. To do this, the dry components of the mixture were rubbed in an agate mortar, then mixed with a solution of PVDF (NMP:PVDF = 8.5:0.5) and rubbed through a fine mesh (~90 μm). A copper foil 14 μm thickness was coated by the resulting mass with a layer of 100 μm and dried at 80 °C for 30 min. The active layer thickness was reduced from 31 to 15 μm by using calender rolls. After that, 15 mm (in diameter) electrodes were cut out and dried at 110 °C in vacuum. The electrodes were mounted in a CR2032 two-electrode disk cell with a lithium counter electrode in argon atmosphere. Celgard 2325 separators were used for the electrical insulation of the electrodes. The base electrolyte was TC-E918, which is a 1 M solution of LiPF_6 in a mixture of EC/PC/DEC/EMC/PA (ethylene carbonate, propylene carbonate, diethyl carbonate, ethyl methyl carbonate, propyl acetate), to which 10 wt.% FEC (Aldrich fluoroethylene carbonate) was added. The charge–discharge curves were measured in the galvanostatic mode on a Neware CT 3008 W-5 V10 mA cycle tester at a current density of 25–100 mA/g. When Li was inserted, the voltage at the studied electrodes relative to the reference electrode was limited by a voltage of 10 mV and, when Li was extracted, by a voltage of 2 V. Impedance measurements were performed using a Biologic VSP modular potentiostat/galvanostat in the frequency range ν from 100 kHz to 0.01 Hz, and the amplitude of the alternating voltage was 7 mV.

The ZView software (Scribner Associates Inc., Southern Pines, NC, USA) was used to calculate the impedance spectra. In this case, the exponents n were fixed; to find the

values of A_1 , A_2 , and A_3 , n was chosen in the range of 0.65–0.85; for A_4 , it was within the range of 0.45–0.63. The deviation of these indices from 1 and from 0.5 are associated with various reasons, for example, with the rough surface of the electrode [18] or the layered structure of the solid phase SEI film [19–21]. The agreement between the experimental and calculated data was achieved by varying the remaining parameters of the equivalent circuit. The relative error of the calculated parameters was 0.2–8.6%.

3. Results

Preliminary experiments showed that the addition of 3 wt.% FEC did not give a positive effect, while 10 wt.% FEC addition led to a decrease in the degradation rate (Figure 1).

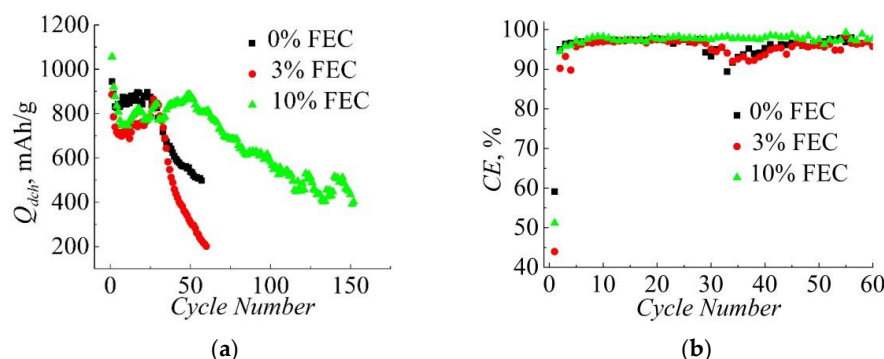


Figure 1. Dependence of the discharge capacity (a) and Columbic efficiency (b) on the cycle number for composite anodes in the form of pellets. The current density during the first lithiation was 25 mA/g, during the first delithiation, and in subsequent cycles 50 mA/g.

The sample with 10 wt.% FEC (1050 mAh/g) has the highest value of specific capacity at the first cycle. For 0 wt.% and 3 wt.% FEC, the capacity values are 940 and 880 mAh/g, respectively. During the first 3–7 cycles there is a drop in capacity, then the samples come to a “shelf”. For the next 20–50 cycles, there is an increase in specific capacity values; however, after 30 cycles there is a degradation of the electrode with 0 wt.% and 3 wt.% FEC. For the sample with the highest FEC content in the electrolyte, the capacity values slowly decrease, but only after 60 cycles. For cycle 60, the specific capacity values for electrodes with 0, 3, and 10 wt.% FEC are 500, 210, and 810 mAh/g, respectively. According to [22], the FEC content lower than 10 wt.% is not enough to obtain a stable SEI layer, which leads to faster degradation of the anode. It is also worth noting that the addition of 10 wt.% has a positive effect on the reversibility of the cycling process (Figure 1b). The values of columbic efficiency are 97–98% in contrast to the samples with minimum FEC content and without it (95–96%).

Further experiments were carried out on samples fabricated by slurry technology. The influence of FEC on the characteristics of the negative electrodes was demonstrated by comparison of two pairs of electrodes A and B in cells with a base electrolyte and with the same electrolyte to which 10 wt.% FEC was added. Table 1 and Figure 2 show the performance of the samples.

Table 1. Parameters of samples made by the “slurry” technology.

Compared Pairs	Sample No.	S, cm^2	$m \text{ Si/C, mg}$	$j, \text{mA/g}$	Capacity Retained at the 300th Cycle, $Q_{\text{dch}(300)}/Q_{\text{dch}(1)}$
A	0% FEC		1.67		20%
	10% FEC		1.67		37%
B	0% FEC	1.77	1.50	100	22%
	10% FEC		1.50		32%

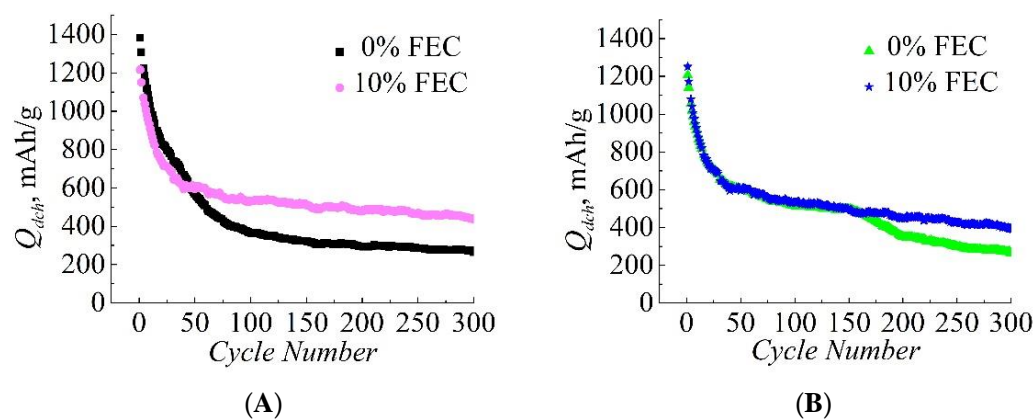


Figure 2. Dependence of the discharge capacity on the cycle number for samples with and without FEC in pairs (A,B).

The samples with FEC degraded slower than those without FEC. At the 300th cycle, their discharge capacity $Q_{dch}(300)$ was 400–450 mAh/g, while for the samples without FEC $Q_{dch}(300)$ was 270 mAh/g, which is ~1.5 times lower and even lower than that of graphite anodes.

The 69% columbic efficiency of the 1st cycle was approximately the same for all four samples. It sharply increased in the second cycle and then increased slowly, reaching a stationary value of 99.9% (Figure 3). Large losses in the 1st cycle were apparently determined by the high surface area of the loose carbon shell [17].

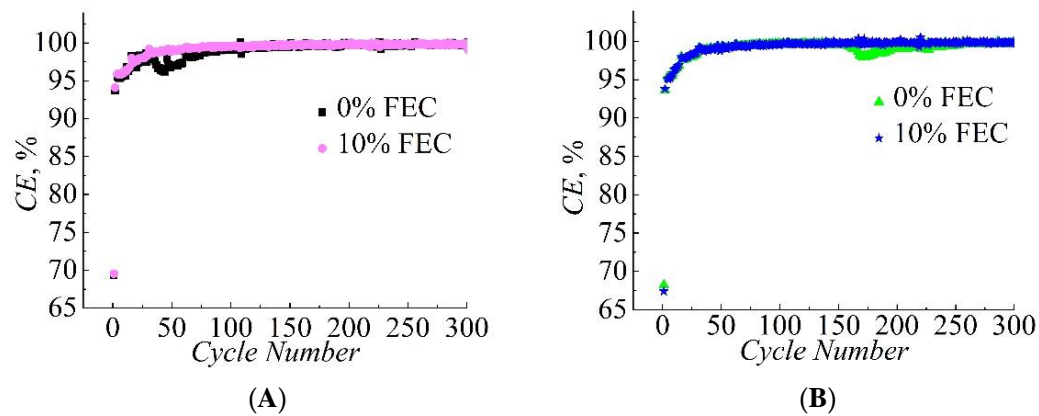


Figure 3. Columbic efficiency versus cycle number for samples in pairs (A,B).

Figure 4 shows the charge–discharge curves of samples in both pairs A and B for 1, 5, 100 and 300 cycles. The curves with and without additives have a similar shape, indicating similar processes. For the electrode pair in Figure 2A, the gained capacity for the sample with 0% FEC is slightly higher than for the samples in Figure 2B. The reason for this is a peculiarity of the shape of the lithiation curve (Figure 4A), which has a gentle section near the potential of 10 mV. With this shape of the curve, even small differences in the resistance of the electrodes lead to significant differences in the gained and given capacity. The increased capacity in the first cycles leads to its significant decrease in the subsequent ones, especially for the samples without FEC.

The dQ/dV plots for the composite Si/C anodes with and without FEC addition to the electrolyte are shown in Figure 5. On the first cycle, all the samples have the same shape of plots with the cathode peak at ~ 0.05 V and the clearly expressed anode peak at 0.43 V. The peak at ~ 0.05 V is due to the lithiation of crystalline Si; the peak at 0.43 V is due to the delithiation of $\text{Li}_{15}\text{Si}_4$ [22]. On cycle 5, the formation of a cathode peak at 0.2 V and anode peaks at ~ 0.3 and 0.5 V occurs. The appearance of these peaks is associated

with the lithiation and delithiation of amorphous silicon [22], which is formed after the first lithiation process. At the same time, the intensity of the peak at 0.43 decreases accordingly. It is worth noting that for samples with FEC, the decrease in the peak intensity is stronger. This may indicate that more crystalline silicon included in the Si/C electrodes was lithiated in the samples with FEC by cycle 5. By cycle 100, the anodic peak at 0.43 disappears, the peak at 0.5 V becomes less pronounced, and this shape of the curves persists in subsequent cycles. It is important to note that during prolonged cycling, starting from cycle 100, the samples with FEC have the smallest changes in the dQ/dV plots, which corresponds to the best preservation of capacity.

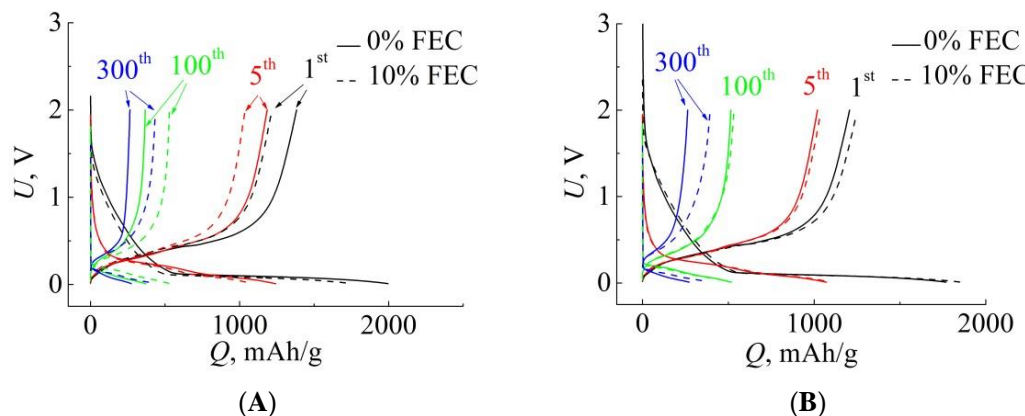


Figure 4. Charge–discharge voltage profiles for samples with and without FEC in pairs (A,B) for 1, 5, 100, 300th cycles. The current density during the lithiation/delithiation of the electrodes was 100 mA/g.

The ability to recharge with different currents was tested after the 300th cycle. The results are presented in Figures 6 and 7. Increase in the current density to $j = 200$ mA/g significantly reduced the discharge capacity, leaving an advantage for the samples with the addition of FEC in the absolute value of Q_{dch} , but not in percentage terms. At $j = 400$ mA/g, the samples with both electrolytes showed almost the same low capacity, while switching to the mode with $j = 100$ mA/g returned the previous Q_{dch} values. The low values of the discharge capacity at $j = 400$ mA/g can be explained by insufficient electrode lithiation at this current density. At lithiation with a lower current density, of course, the discharge capacity will be significantly higher.

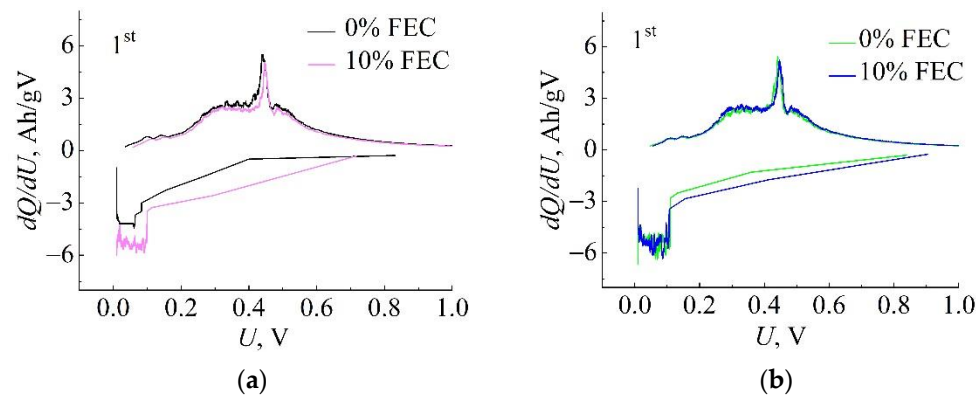


Figure 5. Cont.

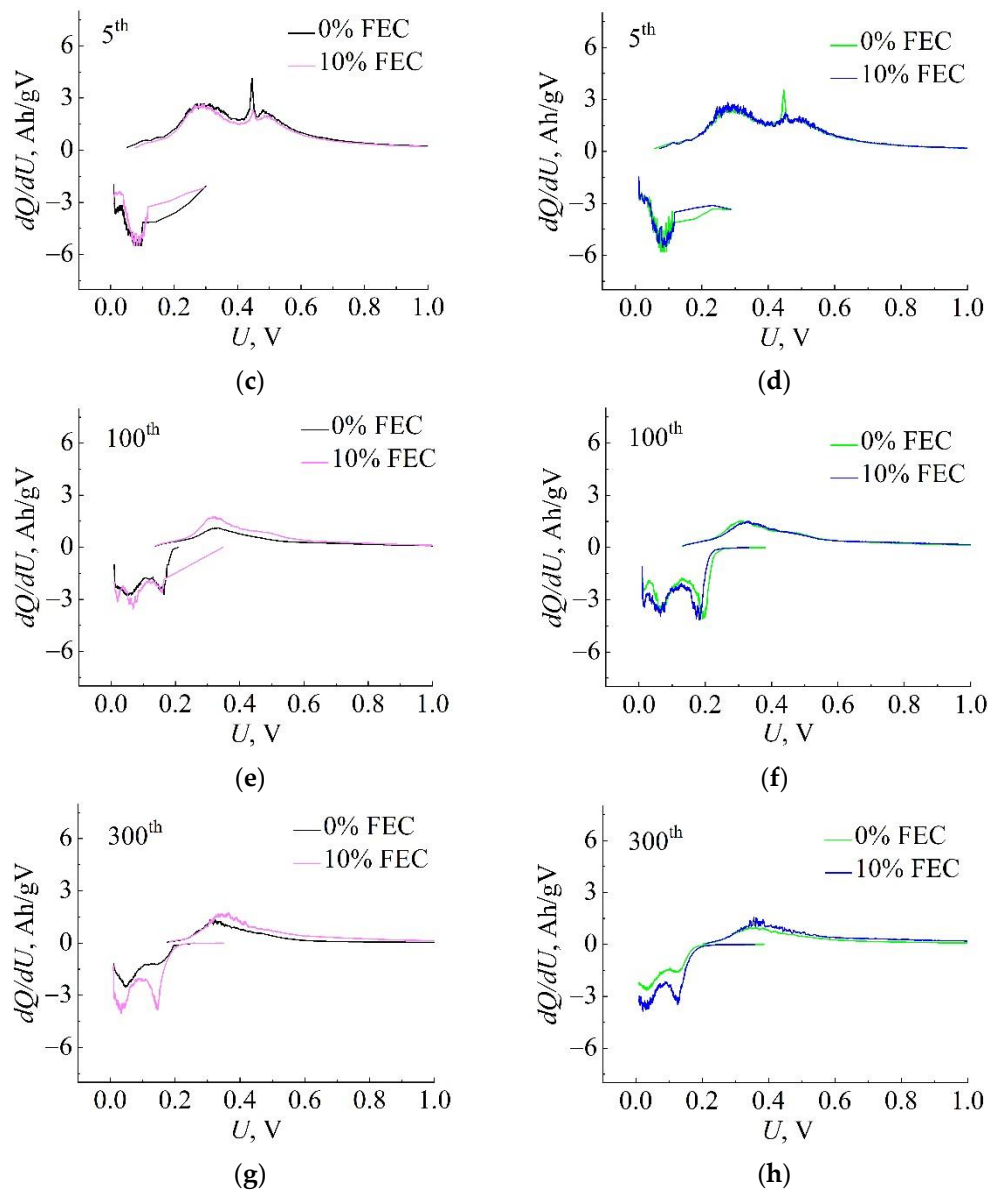


Figure 5. Differential capacity (dQ/dU) plots of Si/C electrodes at different cycle number. The left column compares the samples of pair A (a,c,e,g), and the right compares pair B (b,d,f,h).

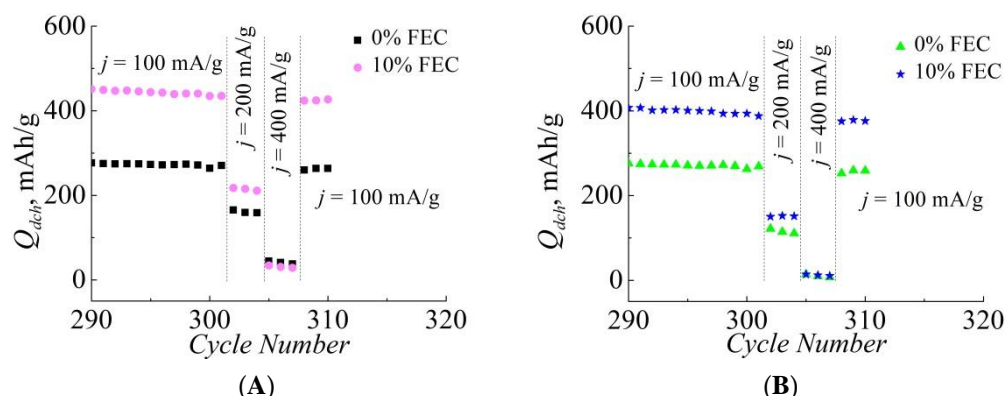


Figure 6. The result of recharging with increased currents after the 300th cycle for the samples in pairs (A,B).

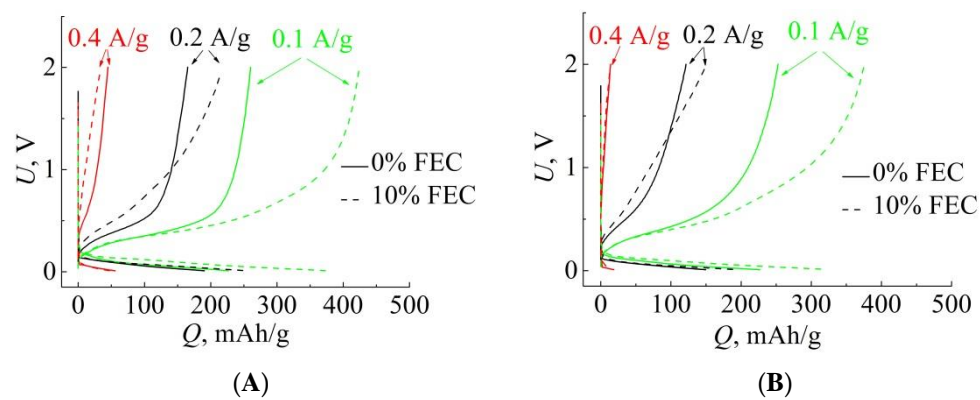


Figure 7. Charge–discharge curves at various rates of electrodes in pairs (A,B) after the 300th cycle.

The impedance of all samples was measured in a charged (completely lithiated) state: the first measurement on the 3rd cycle, subsequent measurements every 15 cycles. After the current was switched off, the cells were kept for a sufficiently long time, during which a stationary potential $U = 0.14 \pm 0.01$ V was established on them. Figure 8 shows the Nyquist plots for five selected cycles. Since the surface area of all samples is the same, only the resistance (not specific value) is given along the x-y axes. For the early cycles, the impedance in the high-frequency range of samples with FEC was greater than those without FEC addition, and became comparable for both type of samples in the high-frequency range after long cycling. It should be noted that after long cycling the corresponding semicircles became flatter, which some authors explain by the emerging inhomogeneity of the SEI [12].

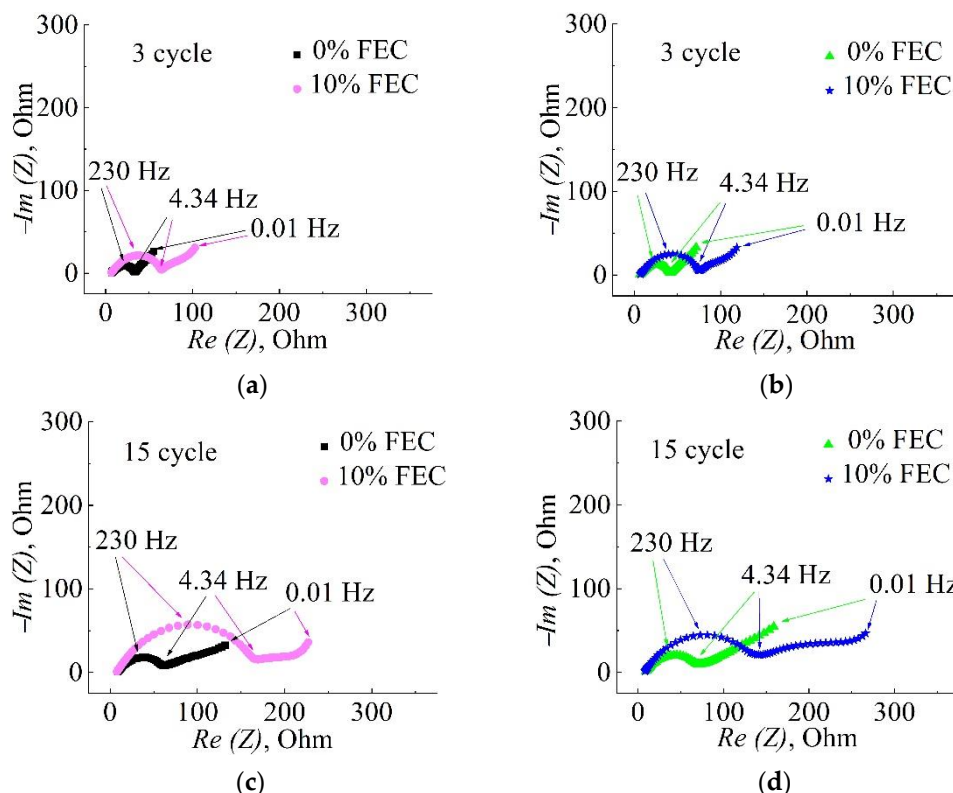


Figure 8. *Cont.*

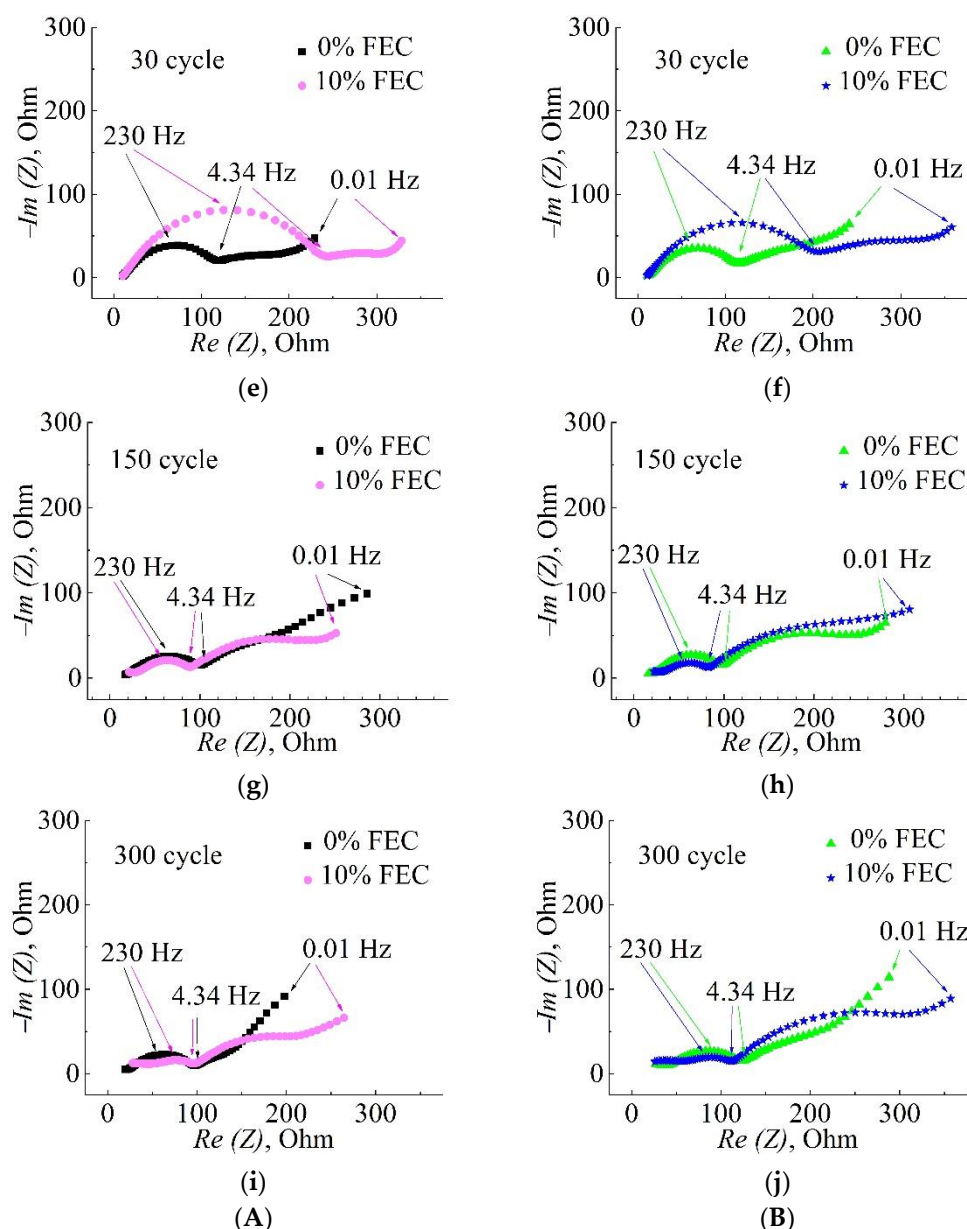


Figure 8. Transformation of the Nyquist plot shape in the process of cycling. Spectra for 3, 15, 30, 150 and 300th cycles are shown: left column for pair (A) (a,c,e,g,i); right column for pair (B) (b,d,f,h,j).

Based on the spectra obtained, the following equivalent electrical circuit consisting of 5 series-connected elements was proposed (Figure 9).

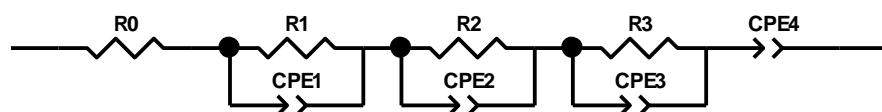


Figure 9. Equivalent electrical circuit simulating the impedance spectra of Si/C electrodes.

The first element R_0 represents all the ohmic resistances of the system, including the resistance of the electrolyte. The next three blocks are parallel combinations of resistance and element with a constant phase shift ($R_1 \parallel \text{CPE}_1$), ($R_2 \parallel \text{CPE}_2$) and ($R_3 \parallel \text{CPE}_3$). The first two blocks model a semicircle, which is in the region between 100 kHz and 4 Hz and represents the superposition of one semicircle on another. The data obtained indicate the existence of two processes that govern charge transfer through the solid electrolyte layer. Thus, SEI

is modeled by two parallel chains, $(R_1 \parallel \text{CPE}_1)$ and $(R_2 \parallel \text{CPE}_2)$. It should be noted that a high-frequency semicircle is inherent in many lithium electrode systems in which there is a passive SEI film [19,23,24]. The third block $(R_3 \parallel \text{CPE}_3)$ models a semicircle at a lower frequency, which is responsible for the process of charge transfer between the electrode and electrolyte and determines the capacitance of the electrical double layer. Indeed, the capacitance A_3 exceeds the capacitances A_1 and A_2 by 3 orders of magnitude, which also agrees with the data of works [25–27]. The last element (CPE_4) models a low-frequency linear section (Warburg impedance), which characterizes the diffusion of lithium atoms in the volume of the solid phase of the electrode.

The impedance of an element with a constant phase shift is calculated by the formula:

$$Z_{\text{CPE}} = i/A \cdot \omega^n,$$

where i is the imaginary unit, $\sqrt{-1}$, $\omega = 2\pi\nu$ is the circular frequency of the measuring signal, and A is a parameter that, depending on the exponent n , can correspond to resistance ($n = 0$), capacitance ($n = +1$), inductance ($n = -1$) and the Warburg impedance coefficient ($n = 0.5$) [28].

The results of the calculation of parameters for the initial and final cycles of samples with and without FEC are summarized in Table 2.

Table 2. Calculated values of the parameters of the equivalent circuit for the impedance spectra in the lithiated state of Si/C electrodes for the 3rd and 300th cycles.

Pair	A				B			
	Sample		0% FEC	10% FEC	0% FEC		10% FEC	
Cycle No.	3	300	3	300	3	300	3	300
R_0 , Ohm	6.6	13.6	6.6	12.5	6.7	11.8	6.8	12.1
R_1 , Ohm	4.8	11.4	4.2	36.8	30.7	31.3	5.9	48.6
A_1 , μF	157.0	8.40	60.1	3.28	68.3	3.26	81.0	3.72
n_1	0.7	0.7	0.8	0.7	0.85	0.7	0.75	0.7
R_2 , Ohm	21.7	71.6	52.4	46.2	4.0	74.2	61.3	47.3
A_2 , μF	88.7	72.3	51.9	88.2	51.4	52.9	46.6	46.3
n_2	0.85	0.7	0.85	0.7	0.8	0.75	0.85	0.8
R_3 , Ohm	6.12	36.4	12.67	115.0	9.14	48.8	16.0	194.0
A_3 , $10^4 \mu\text{F}$	40.72	1.24	7.28	0.52	17.34	0.9	5.23	0.39
n_3	0.7	0.7	0.8	0.65	0.7	0.7	0.8	0.65
A_4 , $\text{Ohm}^{-1} \cdot \text{Hz}^{-n_4}$	0.168	0.052	0.097	0.048	0.133	0.02	0.091	0.040
n_4	0.6	0.63	0.5	0.5	0.6	0.45	0.5	0.5

Figure 10 shows dependencies of the equivalent circuit parameters on the cycle number. The resistances R_1 and R_2 characterizing the SEI layer showed similar trends for both pairs of samples. R_1 was much smaller than R_2 and increased smoothly with the cycle number in the case of both electrolytes. The R_2 value of FEC containing electrolyte first exceeded R_2 of electrolyte without FEC and then became smaller than the latter. The cells with FEC were characterized by the emergence of a maximum at $N = 30$ in the dependence of the resistance on the cycle number $R_2 = f(N)$, which was more pronounced in comparison with the base electrolyte cells. The capacitance A_1 gradually decreased and stabilized at the level of several μF , and A_2 , after a slight drop from the 3rd to 30th cycle, demonstrated a weak and almost synchronous increase for both electrolytes.

For R_3 , which describes the charge transfer resistance across the electrode–electrolyte interface, the greatest difference between the impurity and base electrolyte appeared on cycles with large numbers (100–200). In [22,29], it was shown that, starting from the concentration of 20–25%, the impedance begins to grow, with the electrode showing good performance with a large number of cycles. The reason for this is the formation of large amounts of poly (FEC) and LiF in the composition of SEI. Probably for our electrodes this

effect appears at lower concentrations of FEC. A_3 (double layer capacity) for both sample pairs in the case of FEC addition was significantly lower than that for the samples without FEC, and also approached the values for the base electrolyte at the 30th cycle.

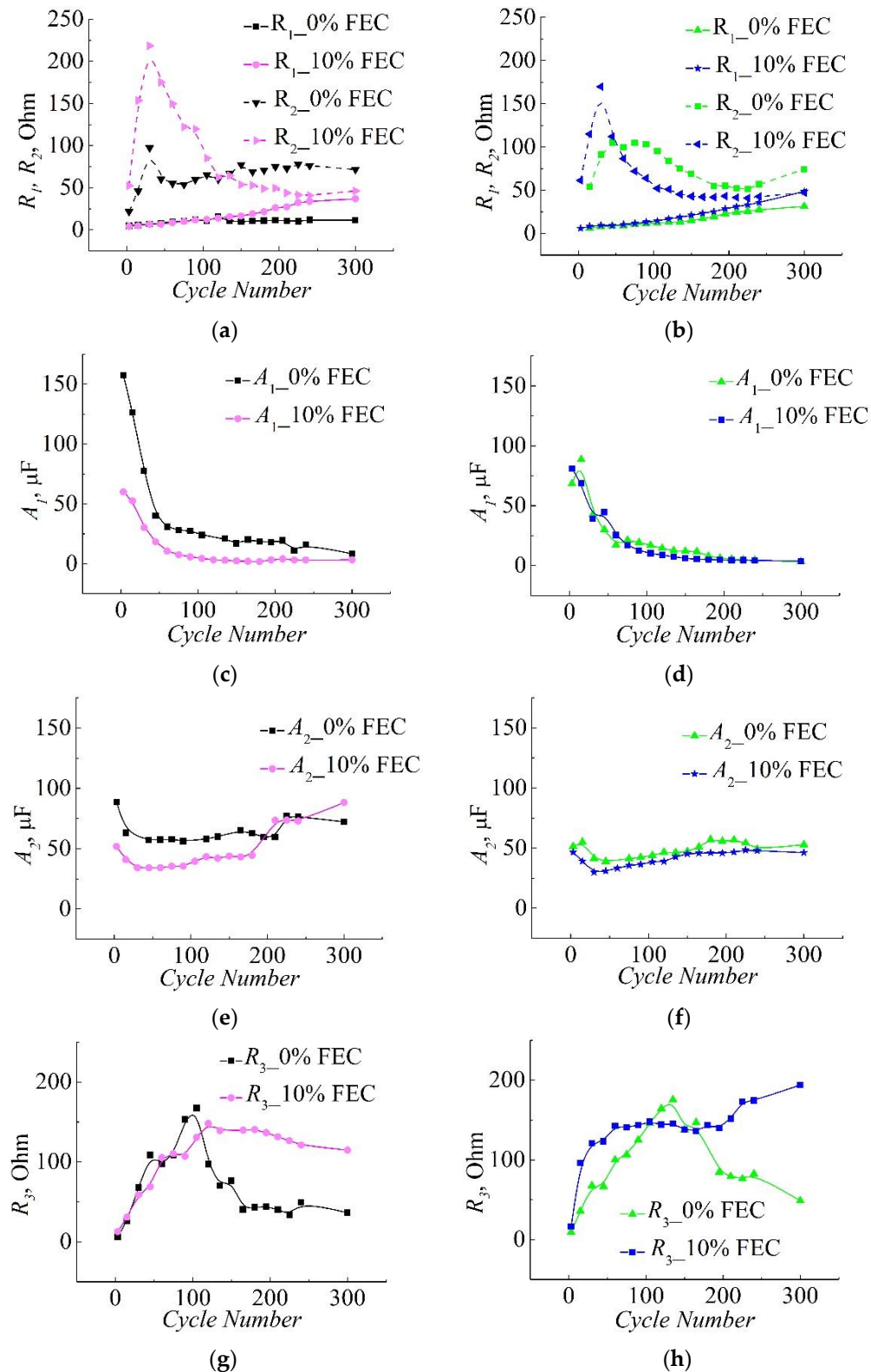


Figure 10. *Cont.*

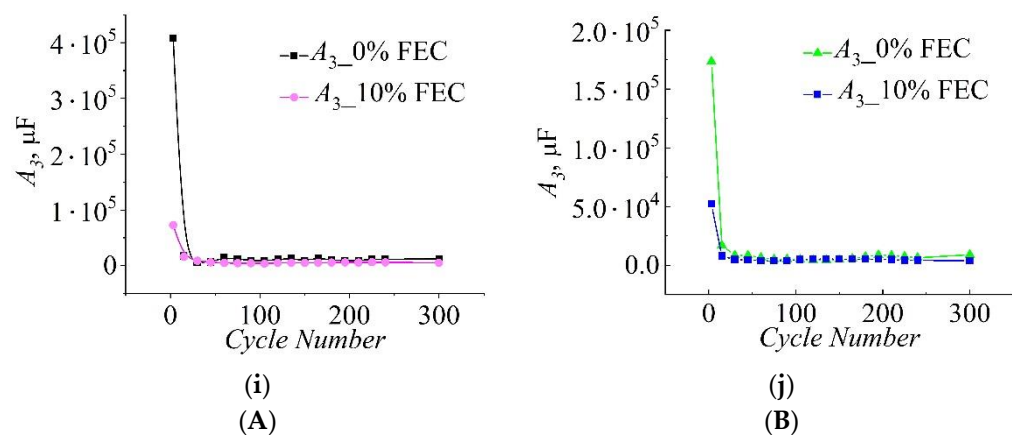


Figure 10. Dependencies of the equivalent circuit parameters on the cycle number for samples with and without FEC. The left column compares the samples of pair (A) (a,c,e,g,i), and the right compares the samples of pair (B) (b,d,f,h,j).

4. Discussion

The SEI layer consists of the reduction products of the organic components of the electrolyte and the lithium-containing salt, in our case, LiPF₆. The decomposition potentials relative to Li/Li⁺ are characterized by the series LiPF₆ > FEC > VC > EC > DEC [26,30]. SEI consists of lithium carbonate Li₂CO₃, lithium alkyl carbonates ROCO₂Li, lithium fluoride LiF, lithium oxide Li₂O, and nonconductive polymers (cross-linked oligomers) [6]. At full lithiation (charge up to 10 mV), the SEI surface is enriched with LiF and Li₂CO₃ [31]. FEC decomposition starts at a potential of 1.3 V [11]. The presence of FEC leads to the formation of more fluorine compounds such as LiF and FEC decomposition products (C-F compounds) as well as salt residues. Thus, the SEI layer resulting from the decomposition of the electrolyte with the addition of FEC contains more inorganic substances than in the case of the base electrolyte. The addition of FEC leads to a change in the composition and organic recovery products.

A feature in performance of Si-containing anodes is the cracking of the material as a result of large volume changes. In this case, destruction of the passivation film SEI can occur. Because of this, with each new cycle, a new SEI is formed, which is expressed in a decrease in the columbic efficiency and ultimately leads to electrode degradation. Therefore, it is required that the SEI film has high coating uniformity, elasticity and stability. Note that, in our samples, after the 30th cycle CE > 99%, which indicates that the formation of a new SEI practically does not occur.

Gain in resistance R₂ in the initial cycles can be explained by a more active process of SEI formation in the electrolyte containing FEC and, apparently, by the formation of a thicker film. This correlates with the drop in capacities A₁ and A₂. With longer cycling, inorganic components are accumulated in the SEI of FEC-containing samples; this provides higher conductivity. A small increase in A₂ may be due to a change in the surface area due to the appearance of Si roughness, or an increase in the porosity of SEI.

The elements of an equivalent circuit modeling impedance are determined by physical processes in a real structure that influence each other. Thus, the evolution of the SEI morphology also affects the structure of the electrical double layer, which changes the rate of electrode processes [32]. It should be noted that, in cycles with N > 120–150, the charge transfer resistance R₃ in the case of FEC presence is higher than that without it. This is consistent with the performance under elevated currents (Figure 6). The lower rate of the Li⁺ ion reduction reaction does not interfere with the retention of higher electrode capacity values (Figure 2), and characterizes SEI as more stable. The lower A₃ double layer capacity in the case of FEC for both pairs A and B could be due to the lower LiPF₆ concentration when 10 wt.% FEC was added to the base electrolyte.

5. Conclusions

It is shown that the addition of FEC influences the capacity and cycling stability of the Si/C composite anode. The effect of cyclic capacity improvement was observed at 10 wt.% FEC addition after 50–150 cycle numbers.

Charge–discharge voltage profiles with and without additives have a similar shape, indicating similar processes. In the dQ/dV plots for samples with FEC, the decrease in the peak intensity is stronger due to more crystalline silicon included in the Si/C electrodes being lithiated in the samples with FEC by cycle 5. During prolonged cycling, starting from 100 cycles, the samples with FEC have the smallest changes in the dQ/dV plots, which corresponds to the best preservation of capacity.

An increase in the resistance in the initial cycles can be explained by a more active process of SEI formation in the electrolyte containing FEC. This correlates with capacity changes. With longer cycling, inorganic components are accumulated in the SEI of FEC-containing samples; this provides higher conductivity and capacity increase as the result.

The experimental data show higher stability during long cycling with 10 wt.% FEC additives; after 300 cycles, the discharge capacity is 1.5 times higher than without FEC addition.

Author Contributions: Conceptualization, A.V.P., A.M.R. and E.V.A.; investigation, A.V.P., A.M.R. and D.A.L.; resources, A.M.R. and M.Y.M.; data curation, A.V.P., A.M.R. and D.A.L.; writing—original draft preparation, E.V.A. and A.V.P.; writing—review and editing, A.V.P., A.M.R., D.A.L., M.Y.M. and E.V.A.; project administration, E.V.A.; funding acquisition, M.Y.M. All authors have read and agreed to the published version of the manuscript.

Funding: This research was funded by the State Task 0040-2019-0012. M.Y.M. thanks to the support of the Ministry of Science and Higher Education of the Russian Federation: Advanced Digital Technologies (contract No. 075-15-2022-311 dated 20 April 2022).

Institutional Review Board Statement: Not applicable.

Informed Consent Statement: Not applicable.

Data Availability Statement: Not applicable.

Acknowledgments: The authors thank Andrei A. Krasilin (Ioffe Institute) for the help with the manuscript preparation.

Conflicts of Interest: The authors declare no conflict of interest.

References

1. Zafar Abbas Manj, R.; Zhang, F.; Ur Rehman, W.; Luo, W.; Yang, J. Toward understanding the interaction within silicon-based anodes for stable lithium storage. *Chem. Eng. J.* **2020**, *385*, 123821. [[CrossRef](#)]
2. Liu, X.; Zhu, X.; Pan, D. Solutions for the problems of silicon–carbon anode materials for lithium-ion batteries. *R. Soc. Open Sci.* **2018**, *5*, 172370. [[CrossRef](#)] [[PubMed](#)]
3. Ashuri, M.; Hea, Q.; Shaw, L.L. Silicon as a potential anode material for Li-ion batteries: Where size, geometry and structure matter. *Nanoscale* **2016**, *8*, 74. [[CrossRef](#)]
4. Jin, Y.; Kneusels, N.-J.H.; Marbella, L.E.; Castillo-Martínez, E.; Magusin, P.C.M.M.; Weatherup, R.S.; Jónsson, E.; Liu, T.; Paul, S.; Grey, C.P. Understanding fluoroethylene carbonate and vinylene carbonate based electrolytes for Si anodes in lithium ion batteries with NMR spectroscopy. *J. Am. Chem. Soc.* **2018**, *140*, 9854–9867. [[CrossRef](#)]
5. Ren, W.-F.; Zhou, Y.; Li, J.-T.; Huang, L.; Sun, S.-G. Si anode for next generation lithium-ion battery. *Curr. Opin. Electrochem.* **2019**, *18*, 46–54. [[CrossRef](#)]
6. Pender, J.P.; Jha, G.; Youn, D.H.; Ziegler, J.M.; Andoni, I.; Choi, E.J.; Heller, A.; Dunn, B.S.; Weiss, P.S.; Penner, R.M.; et al. Electrode degradation in lithium-ion batteries. *ACS Nano* **2020**, *14*, 1243–1295. [[CrossRef](#)]
7. Obrovac, M.N.; Chevrier, V.L. Alloy negative electrodes for Li-ion batteries. *Chem. Rev.* **2014**, *114*, 11444–11502. [[CrossRef](#)]
8. Majdi, H.S.; Latipov, Z.A.; Borisov, V.; Nedorezova, O.Y.; Kadhim, M.M.; Suksatan, W.; Khlewee, I.H.; Kianfar, E. Nano and battery anode: A review. *Nanoscale Res. Lett.* **2021**, *16*, 177. [[CrossRef](#)]
9. Choi, N.-S.; Yew, K.H.; Lee, K.Y.; Sung, M.; Kim, H.; Kim, S.-S. Effect of fluoroethylene carbonate additive on interfacial properties of silicon thin-film electrode. *J. Power Sources* **2006**, *161*, 1254–1259. [[CrossRef](#)]
10. Etacheri, V.; Haik, O.; Goffer, Y.; Roberts, G.A.; Stefan, I.C.; Fasching, R.; Aurbach, D. Effect of fluoroethylene carbonate (FEC) on the performance and surface chemistry of Si-nanowire Li-ion battery anodes. *Langmuir* **2012**, *28*, 965–976. [[CrossRef](#)] [[PubMed](#)]

11. Xu, C.; Lindgren, F.; Philippe, B.; Gorgoi, M.; Björefors, F.; Edström, K.; Gustafsson, T. Improved performance of the silicon anode for Li-ion batteries: Understanding the surface modification mechanism of fluoroethylene carbonate as an effective electrolyte additive. *Chem. Mater.* **2015**, *27*, 2591–2599. [[CrossRef](#)]
12. Matsumoto, T.; Kimur, K.; Nishihara, H.; Kasukabe, T.; Kyotani, T.; Kobayashi, H. Fabrication of Si nanopowder from Si swarf and application to high capacity and low cost Li-ion batteries. *J. Alloys Compd.* **2017**, *720*, 529–540. [[CrossRef](#)]
13. Klett, M.; Gilbert, J.A.; Pupek, K.Z.; Trask, S.E.; Abraham, D.P. Layered oxide, graphite and silicon-graphite electrodes for lithium-ion cells: Effect of electrolyte composition and cycling windows. *J. Electrochem. Soc.* **2017**, *164*, A6095. [[CrossRef](#)]
14. Yao, K.; Zhenga, J.P.; Lianga, R. Ethylene carbonate-free fluoroethylene carbonate-based electrolyte works better for freestanding Si-based composite paper anodes for Li-ion batteries. *J. Power Sources* **2018**, *381*, 164–170. [[CrossRef](#)]
15. Pathak, A.D.; Samanta, K.; Sahu, K.K.; Pati, S. Mechanistic insight into the performance enhancement of Si anode of a lithium-ion battery with a fluoroethylene carbonate electrolyte additive. *J. Appl. Electrochem.* **2021**, *51*, 143–154. [[CrossRef](#)]
16. Astrova, E.V.; Ulin, V.P.; Parfeneva, A.V.; Voronkov, V.B. Fluorocarbon carbonization of nanocrystalline silicon. *Tech. Phys. Lett.* **2019**, *45*, 664–667. [[CrossRef](#)]
17. Astrova, E.V.; Ulin, V.P.; Parfeneva, A.V.; Rumyantsev, A.M.; Voronkov, V.B.; Nashchekin, A.V.; Nevedomskiy, V.N.; Koshtyal, Y.M.; Tomkovich, M.V. Silicon–carbon nanocomposites produced by reduction of carbon monofluoride by silicon. *J. Alloys Compd.* **2020**, *826*, 154242. [[CrossRef](#)]
18. Retter, U.; Lohse, H. Electrochemical impedance spectroscopy. In *Electroanalytical Methods: Guide to Experiments and Applications*, 2nd ed.; Scholz, F., Ed.; Springer: Berlin/Heidelberg, Germany, 2010; pp. 159–176.
19. Umeda, M.; Dokko, K.; Fujita, Y.; Mohamedi, M.; Uchida, I.; Selman, J.R. Electrochemical impedance study of Li-ion insertion into mesocarbon microbead single particle electrode: Part I. Graphitized carbon. *Electrochim. Acta* **2001**, *47*, 885–890. [[CrossRef](#)]
20. Aurbach, D.; Weissman, I.; Schechter, A.; Cohen, H. X-ray photoelectron spectroscopy studies of lithium surfaces prepared in several important electrolyte solutions. A comparison with previous studies by Fourier transform infrared spectroscopy. *Langmuir* **1996**, *12*, 3991–4007. [[CrossRef](#)]
21. Wang, C.; Appleby, A.J.; Little, F.E. Electrochemical impedance study of initial lithium ion intercalation into graphite powders. *Electrochim. Acta* **2001**, *46*, 1793–1813. [[CrossRef](#)]
22. Nguyen, C.C.; Lucht, B.L. Comparative study of fluoroethylene carbonate and vinylene carbonate for silicon anodes in lithium ion batteries. *J. Electrochem. Soc.* **2014**, *161*, A1933. [[CrossRef](#)]
23. Churikov, A.V.; Pridatko, K.I.; Ivanishchev, A.V.; Ivanishcheva, I.A.; Gamayunova, I.M.; Zapsis, K.V.; Sycheva, V.O. Impedance spectroscopy of lithium-tin film electrodes. *Russ. J. Electrochem.* **2008**, *44*, 550–557. [[CrossRef](#)]
24. Aurbach, D.; Gamolsky, K.; Markovsky, B.; Salitra, G.; Gofen, Y.; Heider, U.; Oesten, R.; Schmidt, M. The study of surface phenomena related to electrochemical lithium intercalation into Li_xMO_y host materials (M = Ni, Mn). *J. Electrochem. Soc.* **2000**, *147*, 1322. [[CrossRef](#)]
25. Ivanishchev, A.V.; Churikov, A.V.; Ivanishcheva, I.A.; Zapsis, K.V.; Gamayunova, I.M. Impedance spectroscopy of lithium–carbon electrodes. *Russ. J. Electrochem.* **2008**, *44*, 510–524. [[CrossRef](#)]
26. Evschik, E.Y. Silicon-Based Anode Materials for Lithium-Ion Batteries. Ph.D. Thesis, IHTE UB RAS, Yekaterinburg, Russia, 21 December 2016. Available online: http://www.ihte.uran.ru/?page_id=7307 (accessed on 18 July 2022). (In Russian).
27. Kulova, T.L.; Pleskov, Y.V.; Skundin, A.M.; Terukov, E.I.; Kon'kov, O.I. Lithium intercalation into amorphous-silicon thin films: An electrochemical-impedance study. *Russ. J. Electrochem.* **2006**, *42*, 708–714. [[CrossRef](#)]
28. Stoynov, Z.B.; Grafov, B.M.; Savova-Stoynov, B.S.; Elkin, V.V. *Electrochemical Impedance*; Nauka Publisher: Moscow, Russia, 1991; pp. 12–51. (In Russian)
29. Wang, W.; Yang, S. Enhanced overall electrochemical performance of silicon/carbon anode for lithium-ion batteries using fluoroethylene carbonate as an electrolyte additive. *J. Alloys Compd.* **2017**, *695*, 3249. [[CrossRef](#)]
30. Zhang, X.R.; Kostecki, R.; Richardson, T.J.; Pugh, J.K.; Ross, P.N. Electrochemical and infrared studies of the reduction of organic carbonates. *J. Electrochem. Soc.* **2001**, *148*, A1341. [[CrossRef](#)]
31. Chan, C.K.; Ruffo, R.; Hong, S.S.; Cui, Y. Surface chemistry and morphology of the solid electrolyte interphase on silicon nanowire lithium-ion battery anodes. *J. Power Sources* **2009**, *189*, 1132–1140. [[CrossRef](#)]
32. Lukomsky, Y.Y.; Gamburg, Y.D. *Physicochemical Foundations of Electrochemistry*; ID Intellect: Dolgoprudny, Russia, 2008; pp. 203–207. (In Russian)